



Full length article

Tunable first order transition in $\text{La}(\text{Fe,Cr,Si})_{13}$ compounds: Retaining magnetocaloric response despite a magnetic moment reduction

Luis M. Moreno-Ramírez^a, Carlos Romero-Muñiz^b, Jia Yan Law^a, Victorino Franco^{a,*}, Alejandro Conde^a, Iliya A. Radulov^c, Fernando Maccari^c, Konstantin P. Skokov^c, Oliver Gutfleisch^c

^a Dpto. Física de la Materia Condensada, ICMSE-CSIC, Universidad de Sevilla, P.O. Box 1065, 41080, Sevilla, Spain

^b Dpto. Física Teórica de la Materia Condensa, Universidad Autónoma de Madrid, E-28049, Madrid, Spain

^c Institut für Materialwissenschaft, TU Darmstadt, 64287, Darmstadt, Germany



ARTICLE INFO

Article history:

Received 24 May 2019

Received in revised form

13 June 2019

Accepted 14 June 2019

Available online 17 June 2019

Keywords:

Magnetocaloric effect

ABSTRACT

Materials with a large magnetocaloric response require a large magnetic moment. However, we show in this paper that it is possible to retain both the isothermal entropy change and the adiabatic temperature change even using dopants that reduce the magnetic moment of the parent alloy, provided that the first order character of the transition is enhanced. In this work, a combination of first-principles calculations, experimental determination of the magnetocaloric response (direct and indirect) as well as a new criterion to determine the order of the phase transition are applied to Cr-doped $\text{La}(\text{Fe,Si})_{13}$ compounds. Despite a reduction in magnetic moment, the magnetocaloric response is retained up to $x \approx 0.3$ in $\text{LaFe}_{11.6-x}\text{Cr}_x\text{Si}_{1.4}$. Unlike other transition metal dopants, Cr occupy 8b sites and couple antiferromagnetically to Fe atoms. The cross-over of first to second order transition is achieved for a Cr content of $x = 0.53$, larger in comparison to other dopants (e.g. Ni or Mn). A direct relation between the first order character and the hysteresis is observed.

© 2019 Acta Materialia Inc. Published by Elsevier Ltd. All rights reserved.

1. Introduction

Magnetocaloric (MC) materials for room temperature applications require a large magnetic moment that exhibits a strong temperature and field dependence [1]. Therefore, one natural approach to enhance the magnetocaloric response is to increase the magnetic moment of the alloy or compound. However, the temperature change of magnetization does not relate directly to the magnitude of the moment but it depends on the characteristics of the phase transition. In the most general case, however, doping a certain material does not significantly change the details of the transition and, therefore, an increase in the moment will translate into an increase of the magnetocaloric response. However, once the character of the transition is altered, this intuitive relation no longer holds. This is particularly true for compounds that are close to the separation between first and second order phase transition (i.e., the composition of the critical point of the second order phase

transition). In these cases, we will show that the magnetocaloric response can remain essentially constant despite a reduction in the magnetic moment, leading to alternative ways of tackling the optimization of the materials.

$\text{La}(\text{Fe,Si})_{13}$ compounds are one of the most promising families of magnetocaloric materials [1–3]. They are based on abundant, non-critical and non-contaminant elements and exhibit a large MC response with small hysteresis [4–6] and soft magnetic behavior [7]. For $\text{La}(\text{Fe,Si})_{13}$ compounds, their MC effect is attributed to their itinerant-electron metamagnetic transition [3] at low magnetic fields above the Curie temperature (from para-to ferro-magnetic state). This transition is found to be of first order type (FOPT) with associated volume change of around 1% though the crystal symmetry remains unaltered (magneto-elastic transition).

It is well known that a FOPT is defined by the existence of a discontinuity in the first derivative of the free energy with respect to a thermodynamic variable (like magnetization), while a second order phase transition (SOPT) is associated to a discontinuity in the second derivative [8]. SOPT MC materials present lower responses than those of FOPT MC materials, though the former exhibit a larger temperature span and have a reversible character, avoiding the

* Corresponding author.

E-mail address: vfranco@us.es (V. Franco).

hysteresis that accompanies FOPT MC materials [9]. One of the goals for the development of MC materials is to combine the pros from both types of materials: large response without associated hysteresis. Consequently, the search of compounds is currently focused at the intermediate point between both categories of MC materials [10,11]. The family of $\text{La}(\text{Fe},\text{Si})_{13}$ compounds is a good example of this search for the critical point of the transition, as it can exhibit mixed characters of FOPT and SOPT by compositional variations [12,13].

The MC response of $\text{La}(\text{Fe},\text{Si})_{13}$ compounds is the largest around 200 K. For tuning it for room temperature applications, hydrogenation of the sample shifts the transition temperature to temperatures above room temperature (around 340 K) without a significant decrease of the MC response. In addition, very fine tuning of the transition temperature is attained by using different dopants (mainly, rare earths substitution to La or transition metals (TM) to Fe) [14–16]. Moreover, for technological applications, it is also desirable to produce a series of compounds with a distribution of transition temperatures [17] or reduced associated hysteresis [18]; both can be achieved by doping. Elements on the left side of Fe in the periodic table can be employed, being Mn the most extensively studied [6,14,19] though at the expense of lowered MC response and alteration of FOPT to SOPT. Cr addition also leads to a reduction of the transition temperatures in TM-based compounds, being Cr a possible alternative dopant to Mn that minimizes the difficulties in materials preparation (Mn vaporizes or oxidizes easily).

In this work, we show that the MC response (either ΔS_T and ΔT_S) remains essentially constant up to a Cr content of $x \approx 0.3$, though the magnetic moment is significantly reduced. Both experiments and Density Functional Theory (DFT) calculations show that the NaZn_{13} -type crystal structure [20] is unaltered by Cr incorporation. However, in contrast with previously studied dopants such as Co [21] or Ni [13], Cr atoms are found to preferably occupy 8b sites and are antiferromagnetically coupled to Fe atoms. Making use of the recently developed field dependence MC analyses [12,22], the order of phase transitions for the studied series is successfully determined and compared to the results of Banerjee's criterion [23]. According to the results, a non-monotonic evolution of the order of phase transition with increasing Cr content is found (increasing the FOPT character for low Cr concentrations), in agreement with the observed thermal and magnetic hysteresis. Moreover, these analyses aid further estimation of the critical SOPT-FOPT composition, being $x = 0.53$ (larger than previously reported for similar compounds [24] and comparable to other transition metal dopants [13,14]).

2. Experimental

$\text{LaFe}_{11.6}\text{Si}_{1.4}$ compound, which was reported that it underwent a FOPT, was chosen as the parent composition [12]. For each alloy with nominal compositions $\text{LaFe}_{11.6-x}\text{Cr}_x\text{Si}_{1.4}$ ($x = 0$ up to 0.6) 5 g of material were produced by induction melting from pure elements. To remove possible oxides in the elements, La was initially melted by arc melting prior to induction melting with other elements. The ingots were then further segmented into different pieces for subsequent suction casting (using a rectangular mold of $10 \times 4 \times 0.5 \text{ mm}^3$). A 9 wt % excess of La was also added to compensate its vaporization during the melts. Suction casted samples were then annealed (wrapped in Mo foil and sealed in quartz tubes) in a resistive tube furnace at different temperatures for 48 h to obtain high amounts of the desired NaZn_{13} -type structure (subsequently denoted as 1:13 phase). The use of suction casting drastically reduced the annealing process from weeks to days [13].

Microstructural characterization and average bulk compositional quantification of the samples were performed using a Philips XL30 FEG scanning electron microscope equipped with energy-dispersive X ray system (SEM/EDX). The X-ray diffraction (XRD) of the pulverized samples were collected at room temperature using a Stoe Stadi P instrument in transmission mode with Molybdenum $K\alpha_1$ radiation ($\lambda = 0.70930 \text{ \AA}$). Rietveld refinement of the XRD patterns was performed using TOPAS 6.0 software.

Magnetic moment measurements were performed with a vibrating sample magnetometer. The magnetic field was applied along the length of the suction casted plates to minimize contributions from the demagnetizing factor. ΔS_T was calculated numerically from isothermal specific moment (σ) curves measured at different temperatures using Maxwell relation:

$$\Delta S_T(T, H) = \mu_0 \int_0^H \left(\frac{\partial \sigma}{\partial T} \right)_H dH', \quad (1)$$

where the initial magnetic field is chosen as 0. ΔT_S was directly measured in a home-built experimental set-up whereby the sample was thermally isolated to ensure adiabatic conditions during the variation of the magnetic field (more details in Ref. [25]). This device allows us to also characterize the time evolution of the temperature close to the phase transition. As FOPT MC materials can exhibit thermal hysteresis, a discontinuous protocol for erasing the thermal and magnetic history of the samples was performed [26,27]. The field dependence exponent n [28] was calculated from ΔS_T data as:

$$n(T, H) = \frac{d \ln(\Delta S_T)}{d \ln(H)}. \quad (2)$$

Density Functional Theory (DFT) calculations were performed to unveil the structural, electronic and magnetic properties of the $\text{LaFe}_{11.6-x}\text{Cr}_x\text{Si}_{1.4}$ series at atomic-scale, using the VASP code [29]. The one-electron wave functions were expanded in a set of plane waves with a kinetic energy lower than 335 eV [13,30,31]. The projected augmented wave method [32,33] was employed to construct the pseudopotentials of all species involved while the Perdew-Burke-Ernzerhof (PBE) functional [34] was chosen to reproduce the electronic exchange and correlation. As a first step, the four constituent metallic elements were separately tested by calculating simple bulk structures to ensure a good agreement of the obtained lattice parameters and bulk moduli.

The equilibrium geometries of all analyzed compounds were obtained after structural optimizations, which utilize a conjugate gradient algorithm till the forces upon atoms were smaller than 0.005 eV/\AA while each self-consistent electronic loop converged with a tolerance better than 10^{-6} eV . All calculations were initialized from the same parent unit cell with cubic symmetry (space group Fm-3c, crystal structure NaZn_{13}) and a lattice parameter of 11.488 \AA . All the atoms were allowed to relax to find their equilibrium positions and there were no restrictions imposed in the volume cell during the relaxation process. The minimal distortions found in the unit cells after the geometrical optimization indicate that the original cubic symmetry is preserved upon Cr incorporation (see Sec. 3.2 for further crystallographic details). In the calculations, the reciprocal space was sampled using a Γ -centered $3 \times 3 \times 3$ Monkhorst-Pack grid [35]. For exploration of the magnetic and electronic properties, all calculations were performed with collinear spin polarization and the Vosko-Wilk-Nusair interpolation [36] was used to resolve the on-site magnetism at atomic level. Due to the strong ferromagnetism in these compounds, it is necessary to start from an initial configuration of high magnetic

moment: $3.5 \mu_B$ per Fe atom and -3.5 or $+3.5 \mu_B$ per Cr atom were used in this work to obtain the antiferromagnetic or ferromagnetic solutions, respectively. Both the magnetic and electronic features were evaluated using a thinner k -point grid of $5 \times 5 \times 5$ and a Gaussian broadening of 0.1 eV, starting from the pre-converged structures.

3. Results and discussion

3.1. Structural characterization

BSE (Back Scattering Electron) images of the $\text{LaFe}_{11.6-x}\text{Cr}_x\text{Si}_{1.4}$ series after annealing are shown in Fig. 1. Different annealing temperatures were used for different Cr contents for the phase optimization of 1:13 phase, which is highly desired for the large MC response in these compounds. It is found that the required annealing temperatures for maximum amounts of 1:13 have significantly increased with Cr incorporation. Bright spots correspond to $\text{La}_1\text{Fe}_7\text{Si}_1$ or La_3Si_2 phase (P4/nmm and P4/mbm, respectively), dark ones to α -Fe phase (Im-3m) and the grey ones to 1:13 phase (Fm-3c). For all studied compositions, BSE images show a homogenous structure with the 1:13 phase as the main phase. Almost negligible α -Fe impurities were observed for samples with Cr contents up to $x = 0.42$. For samples up to $x = 0.21$, some small black spots can be observed that correspond to shape irregularities (secondary electrons images corroborate this). Small $\text{La}_1\text{Fe}_7\text{Si}_1/\text{La}_3\text{Si}_2$ amounts can be also noted, which could arise from the excess La from the initial element mixture. However, this excess prevents the formation of large amounts of α -Fe. For Cr contents larger than $x = 0.35$, the La_3Si_2 phase is formed while, for smaller contents, the typical $\text{La}_1\text{Fe}_7\text{Si}_1$ phase is obtained. The α -Fe phase fraction becomes more noticeable with increasing Cr concentration though the high 1:13 phase fraction for $x = 0.56$ sample shows an extension of the solid solubility limit previously ascribed to Cr (for a Cr content close to 0.5 we reach 87 wt% of 1:13 phase, while only 73% was achieved in Ref. [37]). A further compositional examination of the secondary phases shows that the Cr/Fe ratio is the highest in α -Fe (e.g. for $x = 0.56$ sample the Cr/Fe ratio is 0.051 and 0.071 for the 1:13 and α -Fe phases, respectively) while there is no Cr in the La_3Si_2 phase. The composition of the 1:13 phase analyzed by EDX is shown in Table 1: the compounds are labeled according to their determined Cr content in 1:13 phase ($x = 0.00, 0.12, 0.21, 0.35, 0.42, 0.47$ and 0.56).

Fig. 2 shows the XRD patterns for the $\text{LaFe}_{11.6-x}\text{Cr}_x\text{Si}_{1.4}$ series. It is observed that the different samples mainly consist of 1:13 phase

and trace amounts of α -Fe (indexed lines); La-rich phases are not clearly detected. Table 1 also shows the lattice parameter of the 1:13 phase ($a_{1:13}$), phase fractions (ξ) and goodness of fit (GoF) obtained from Rietveld refinement of the spectra. GoF values are close to 1 (ideal case) and below 2, indicating a good fitting. For all the compounds, the NaZn_{13} -type structure is retained without a significant modification of the lattice parameter. The amount of α -Fe increases as Cr increases, which is consistent with microstructural analysis by BSE.

3.2. DFT studies

Microscopic crystal structure of the $\text{LaFe}_{11.6-x}\text{Cr}_x\text{Si}_{1.4}$ alloy series was investigated with DFT calculations. All calculations were carried out starting from the same parent unit cell with periodic boundary conditions to reproduce the cubic symmetry of the $\text{LaFe}_{11.6}\text{Si}_{1.4}$ parent sample. All unit cells contained a total of 112 atoms (8 unit formulas) distributed in three nonequivalent Wyckoff positions (8a, 8b and 96i). In the hypothetical LaFe_{13} structure (NaZn_{13} -type), the heavier La atoms would occupy all the 8a positions while Fe atoms would be located either in 8b or 96i sites with full occupancy. In this arrangement, two crystallographic different iron species can be found, labeled as Fe-I (8b) and Fe-II (96i). The structure presented in Fig. 3 shows a distribution of La atoms and Fe-I atoms that follows a cubic CsCl arrangement. Each La atom is surrounded by 24 Fe-II nearest-neighbor atoms, forming a polyhedron that resembles a snub cube. Eight such polyhedra with alternating orientations make up the conventional unit cell, whose lattice parameter is twice the minimum distance of Fe-I–Fe-I (or La–La). On the other hand, the coordination sphere of each Fe-I atoms consists of 12 first neighbors, constituting a near-icosahedron of Fe-II atoms. Therefore, this structure can also be viewed as Fe-II icosahedra stacked in alternating directions, forming a unit cell that contains eight of these icosahedra. In the stable structure of $\text{LaFe}_{11.6}\text{Si}_{1.4}$, a fraction of Fe atoms has been replaced by lighter Si atoms, responsible for the final stabilization. Previous studies [38,39] suggest that the incorporation of Si atoms preferentially or exclusively takes place at 96i sites. Therefore, 13 Fe-II atoms were randomly substituted by Si atoms to closely reproduce the compound composition of $\text{LaFe}_{11.6}\text{Si}_{1.4}$, which serves as starting point ($x = 0$) for the subsequent Cr incorporation. It is worth noting that this unit cell is large enough to reproduce a reasonable random distribution of Si atoms on 96i sites.

To study the effect of Cr substitutional doping in the crystal structure, additional Fe atoms (from 1 to 6) were replaced by Cr

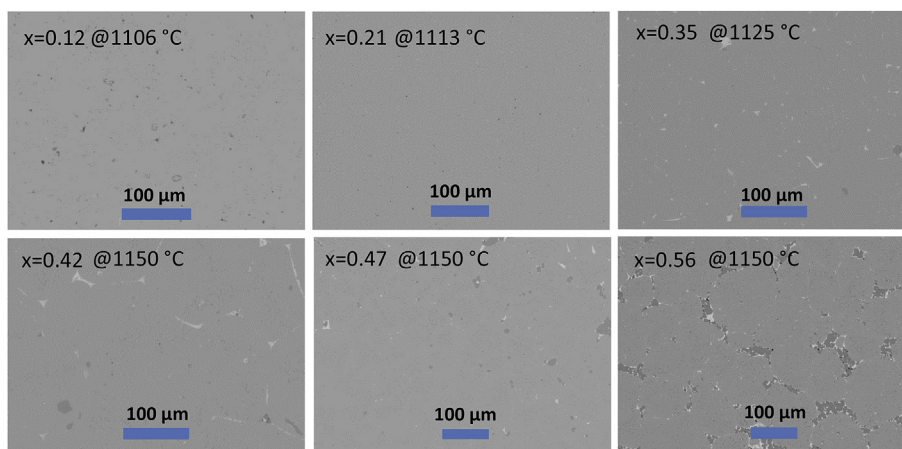


Fig. 1. BSE images of the $\text{LaFe}_{11.6-x}\text{Cr}_x\text{Si}_{1.4}$ samples after annealing at different temperatures (for which maximum 1:13 phase fraction is obtained).

Table 1

Composition of the 1:13 phase determined by EDX analysis and lattice parameter of 1:13 phase, phase fraction and goodness of fit (GoF) determined from Rietveld refinement for the $\text{LaFe}_{11.6-x}\text{Cr}_x\text{Si}_{1.4}$ series.

Compound	Composition [1:13]	$a_{1:13}$ (Å)	$\xi(1:13)$ (wt.%)	$\xi(\alpha\text{-Fe})$ (wt.%)	GoF
x = 0.00	$\text{La}_{1.00(4)}\text{Fe}_{11.5(6)}\text{Si}_{1.40(14)}$	11.478(3)	100	0.0	1.55
x = 0.12	$\text{La}_{1.00(4)}\text{Fe}_{11.3(7)}\text{Cr}_{0.12(2)}\text{Si}_{1.42(14)}$	11.476(3)	100	0.0	1.49
x = 0.21	$\text{La}_{1.00(3)}\text{Fe}_{11.1(5)}\text{Cr}_{0.21(2)}\text{Si}_{1.42(14)}$	11.478(4)	97.7	2.3	1.39
x = 0.35	$\text{La}_{1.00(6)}\text{Fe}_{11.0(7)}\text{Cr}_{0.35(5)}\text{Si}_{1.42(17)}$	11.477(4)	94.9	5.1	1.25
x = 0.42	$\text{La}_{1.00(3)}\text{Fe}_{10.8(5)}\text{Cr}_{0.47(3)}\text{Si}_{1.59(16)}$	11.475(2)	92.8	7.2	1.10
x = 0.47	$\text{La}_{1.00(3)}\text{Fe}_{10.8(7)}\text{Cr}_{0.42(4)}\text{Si}_{1.53(16)}$	11.477(2)	87.5	12.5	1.99
x = 0.56	$\text{La}_{1.00(3)}\text{Fe}_{10.7(5)}\text{Cr}_{0.56(4)}\text{Si}_{1.59(16)}$	11.476(2)	75.5	24.5	1.34

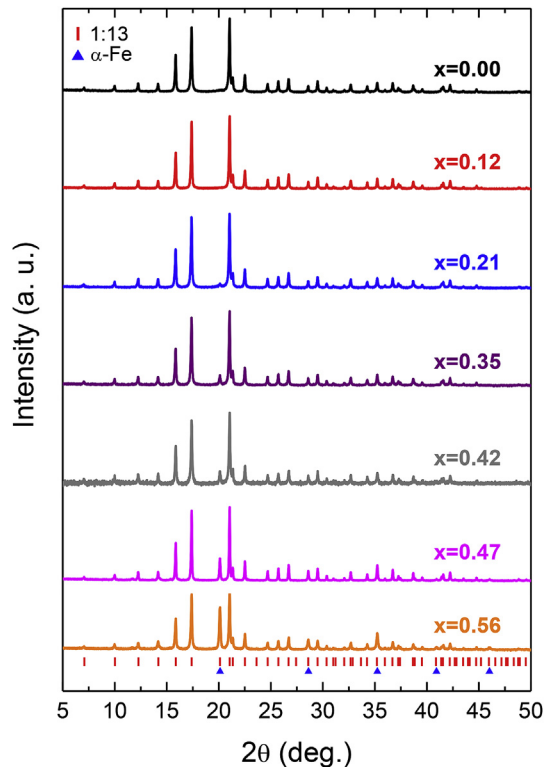


Fig. 2. XRD patterns for the $\text{LaFe}_{11.6-x}\text{Cr}_x\text{Si}_{1.4}$ series. Bragg reflections corresponding to $\alpha\text{-Fe}$ and 1:13 phases are indexed.

atoms, leading to the series of $x = 0.125$, $x = 0.25$, $x = 0.375$, $x = 0.5$, $x = 0.625$ and $x = 0.75$. This enabled a fair comparison with the experimental series of compounds obtained. As the preferential site for the substitution of Cr atoms cannot be assumed a priori, two possibilities were studied: the incorporation at 96i and 8b Wyckoff sites. The calculations point out that the incorporation in Fe–I (8b) sites is clearly more energetically favorable than that at the Fe–II (96i) sites. In particular, we find that Fe–I substitution is stabilized by 0.31 eV per Cr atom in the unit cell with respect to the Fe–II replacement. This is retained for all concentrations studied with similar energy differences. The strong annealing treatment during the synthesis of the samples justifies the selection of the 8b sites for the substitution. In this regard, it is worth noting that Cr atoms display a distinctive behavior compared to other first-row transition metals in the periodic table, despite having a similar atomic size. Especially, Cr dopants have a clear preference to occupy the highly symmetrical 8b sites of Fe–I, rather than the 96i positions of Fe–II, which was the usual substitution observed for Ni [13] or Co [21].

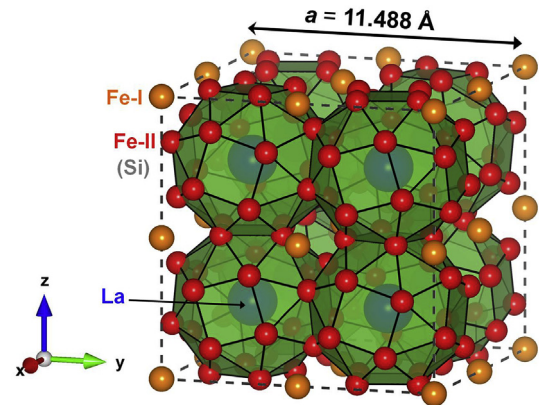


Fig. 3. Perspective view of the unit cell of $\text{LaFe}_{11.6}\text{Si}_{1.4}$ (space group $Fm\text{-}3c$) represented with a ball model displaying the coordination polyhedra of La atoms (blue), which occupy 8a positions. Fe–I atoms (orange) are located on 8b sites while Fe–II atoms (red) and Si atoms (not shown in the figure) distribute randomly on 96i sites. (For interpretation of the references to color in this figure legend, the reader is referred to the Web version of this article.)

The substitution of Cr atoms has a negligible impact on the parent crystal structure. This can be attributed to the preferential occupancy at 8b positions, which possess enough free room to avoid the expansion/compression of the unit cell. The small distortions suffered in the unit cells after Cr substitution are, overall, considered minor for the studied range of concentration. This reveals that the original NaZn_{13} -type crystal structure is preserved upon Cr incorporation. Table 2 shows the lattice parameters and mass densities obtained for the $\text{LaFe}_{11.6-x}\text{Cr}_x\text{Si}_{1.4}$ series. The lattice parameter remains unaltered regardless the concentration of Cr, without showing any relevant tendency, in agreement with XRD results. The same trend is observed for the mass density.

Spin-polarized DFT calculations allow us to get further insight into the magnetic ordering of the alloys, resolving the individual magnetic moments of each atomic species. The parent sample displays a strong ferromagnetic behavior with a total magnetic moment per cell of $24.13 \mu_B$ for $\text{LaFe}_{11.6}\text{Si}_{1.4}$. Using crystallographic data shown in Table 2, the magnetic moment of the cell can be expressed in terms of specific magnetization, leading to a value of 164.4 emu/g . The strong ferromagnetic behavior in the $\text{La}(\text{Fe},\text{Si})_{13}$ compounds arises mainly from the majority Fe–II atoms, which possess an average magnetic moment of $2.24 \mu_B$ per atom, while Fe–I atoms also contribute with a slightly lower value of $1.83 \mu_B$ per atom. In addition, Si and La atoms show a slight anti-parallel coupling with residual magnetic moment per atom of $-0.10 \mu_B$ and $-0.21 \mu_B$ respectively. These findings are in concordance with previous calculations [30,39] and experimental values obtained by neutron scattering [38] and Mossbauer spectroscopy [40].

Table 2
Lattice parameters, mass densities, magnetic moment per unit cell and saturation magnetization obtained with DFT calculations for the $\text{LaFe}_{11.6-x}\text{Cr}_x\text{Si}_{1.4}$ series. The number of atoms of each species per unit cell is also indicated.

Atoms per unit cell					Compound	a	Atomic weight	Density	μ	σ_s
La	FeI	FeII	Cr	Si		(Å)	(g mol ⁻¹ f.u. ⁻¹)	(g cm ⁻³)	(μ_B f.u. ⁻¹)	(emu g ⁻¹)
8	8	83	0	13	$\text{LaFe}_{11.6}\text{Si}_{1.4}$	11.4436	819.781	7.27	24.13	164.4
8	7	83	1	13	$\text{LaFe}_{11.475}\text{Cr}_{0.125}\text{Si}_{1.4}$	11.4395	819.300	7.27	23.46	160.0
8	6	83	2	13	$\text{LaFe}_{11.35}\text{Cr}_{0.25}\text{Si}_{1.4}$	11.4347	818.819	7.28	22.79	155.5
8	5	83	3	13	$\text{LaFe}_{11.225}\text{Cr}_{0.375}\text{Si}_{1.4}$	11.4296	818.338	7.28	22.10	150.8
8	4	83	4	13	$\text{LaFe}_{11.1}\text{Cr}_{0.5}\text{Si}_{1.4}$	11.4236	817.857	7.29	21.43	146.3
8	3	83	5	13	$\text{LaFe}_{10.975}\text{Cr}_{0.625}\text{Si}_{1.4}$	11.4270	817.376	7.28	21.17	144.7
8	2	83	6	13	$\text{LaFe}_{10.85}\text{Cr}_{0.75}\text{Si}_{1.4}$	11.4289	816.895	7.27	20.86	142.6

First-principles calculations to study the changes of the magnetic properties at the atomic level upon progressive Cr incorporation were also performed. A noticeable reduction (approximately 15%) in the total magnetic moment per f.u. (and saturation magnetization) with increasing Cr concentration is shown in Table 2, decreasing from the initial 24.13 μ_B ($x = 0$) to 20.86 μ_B ($x = 0.75$). For that, the atomic on-site magnetic moment distribution collected in Fig. 4 is further studied. The most relevant feature of substitutional Cr dopants is the antiferromagnetic coupling to Fe atoms. No ferromagnetic solution is observed for Cr additions, in agreement with previous calculations on a reduced cell, which also pointed out to the exclusivity of the antiferromagnetic coupling [41]. However, it is remarkable the existence of a stable ferromagnetic solution for low Cr concentration ($x = 0.125$) but only when the Cr atoms are incorporated in 96i sites, which is not the most energetically favorable configuration. Hence, the only stable solution is the one with anti-parallel magnetic coupling between Cr and Fe atoms. This is reflected by the bar charts in Fig. 4, where Fe-I and Fe-II atoms show opposite signs to the other atoms in the compounds, wherein their magnetic moments are represented by different colored bars: Cr (purple), Si (grey), La (blue), Fe-I (orange) and Fe-II atoms (red). Notice that in all these cases

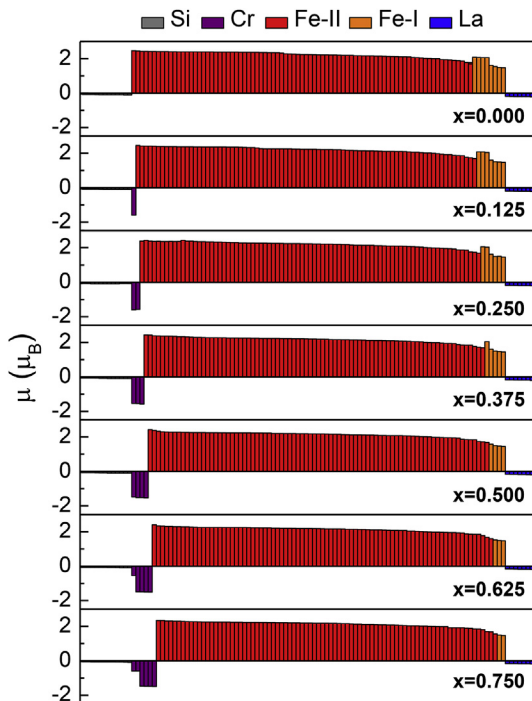


Fig. 4. Atomic on-site resolved magnetic moment obtained with spin-polarized DFT for the 112 atoms of the unit cell in the $\text{LaFe}_{11.6-x}\text{Cr}_x\text{Si}_{1.4}$ compound as a function of Cr content.

the coupling is entirely antiferromagnetic. Cr atoms usually display a magnetic moment of $-1.5 \mu_B$ but for higher Cr content ($x = 0.625$ and $x = 0.75$), the antiferromagnetic coupling weakens and some Cr atoms display a lower value of magnetic moment ($-0.5 \mu_B$). The slight asymmetry between 8b sites is likely a spurious effect due to the absence of a real random distribution of Si atoms on 96i sites.

According to this scenario, the reduction in the total magnetic moment is attributed to the antiferromagnetic coupling of the new Cr atoms incorporated in the crystal lattice. No other relevant changes in the magnetic moment distribution of La, Fe or Si atoms are observed with respect to the original parent sample of $\text{LaFe}_{11.6}\text{Si}_{1.4}$. This strong antiferromagnetic coupling is another distinctive fingerprint of Cr dopants in this system at variance with other similar transition metals, like Co or Ni, which displays only ferromagnetic coupling [13,21,41], or Mn, whose preferential magnetic configuration is not clear [41,42].

Fig. 5 shows the different contributions of the atoms in the unit

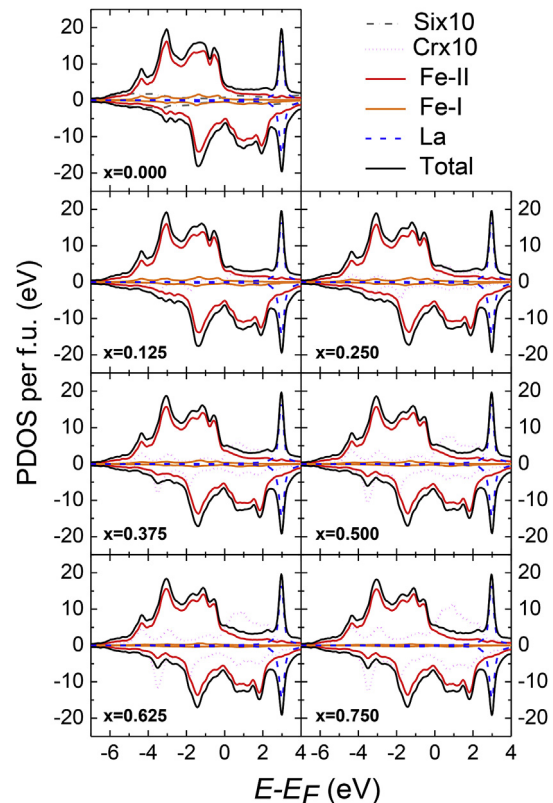


Fig. 5. Evolution of the electronic properties of the $\text{LaFe}_{11.6-x}\text{Cr}_x\text{Si}_{1.4}$ alloy with increasing Cr concentration. Each curve represents the accumulative PDOS of each species (the sum of the PDOS of all atoms of the same class). Notice that Si contribution is only shown for $x = 0$ and it remains unaltered in the other compositions.

cell to the total electronic density of states (DOS). Each curve represents the accumulated projected density of states (PDOS) of each species, that is, the sum of atomic PDOS of atoms belonging to the same class. As expected, the contributions of La and Si atoms are minor and they remain unchanged with Cr substitution. Conversely, the main contribution arises from the Fe atoms, the majority species, especially Fe-II atoms, due to their higher proportion. The presence of Fe-II atoms is responsible for the strong ferromagnetic behavior shown in this material. Notice, for instance, the clear differences between up and down PDOS in $E-E_F \approx -3$ eV or $+2$ eV, which appear in all studied concentrations of Cr. The presence of Cr dopants reveals a distinctive behavior also characterized by a magnetic fingerprint, showing opposite signs of those of Fe-II. This is mainly observed in the down PDOS peaks located at $E-E_F \approx -4$ eV and -2 eV, whose magnitude grows with increasing Cr content. However, it has to be noted that the atomic Cr/Fe ratio is rather low and the main characteristics of the studied series will be essentially those coming from the majority Fe-II atoms, like the strong ferromagnetic ordering in spite of the Cr antiferromagnetic coupling.

3.3. Magnetocaloric properties and characteristics of the phase transition

Fig. 6 shows the temperature dependence (heating and cooling) of the normalized magnetic moment with respect to the value at 100 K for 0.05 T. In this representation, the high temperature values offer information on the amount of α -Fe, which are only evident for higher Cr content, in agreement with the XRD values. The transition temperature shifts to lower temperatures with increasing Cr content. Determining T_{trans} as the temperature for which the derivative of magnetization with respect to temperature is maximum for the cooling curve, a linear trend as a function of the Cr content (rate of

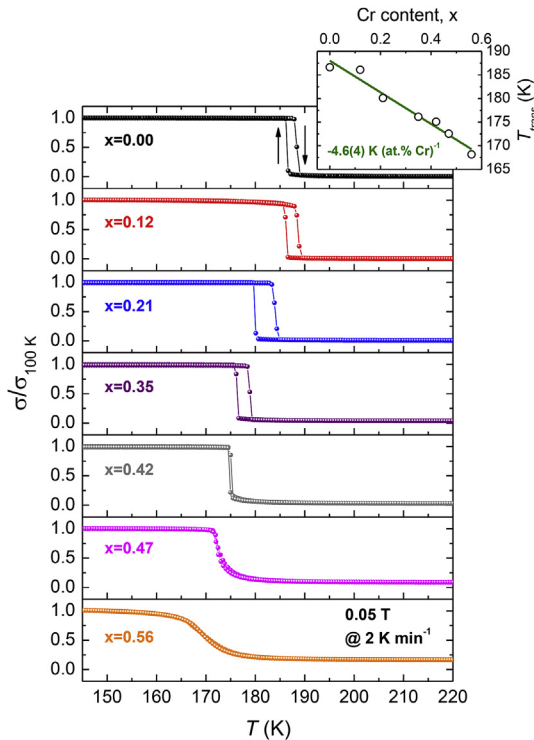


Fig. 6. Temperature dependence of the normalized magnetization with respect to the magnetization at 100 K for a magnetic field of 0.05 T for the $\text{LaFe}_{11.6-x}\text{Cr}_x\text{Si}_{1.4}$ series. Inset: Calculated T_{trans} while cooling as a function of Cr content.

$4.6(4)$ K (at.% Cr) $^{-1}$) is observed, which is further shown in the inset of Fig. 6. This rate of change is smaller than those found in other TM-doped series such as Co [43] or Mn [42]. It is experimentally found that magnetic moment of the 1:13 phase reduces with Cr additions (about 10 emu/g per at. % Cr at around 150 K), in agreement with DFT calculations, though the presence of α -Fe phase prevents any further analysis. Fig. 7 shows the thermal hysteresis (blue curve) obtained from the data presented in Fig. 6 as a function of Cr content. A non-monotonic behavior of the thermal hysteresis as Cr content increases is observed. The maximum value is observed for $x = 0.21$ sample, while hysteresis decreases for higher Cr content, reaching values close to zero for $x = 0.47$ and 0.56 samples. In addition, the magnetic hysteresis (red curve) is analyzed from the magnetization/demagnetization curves at temperatures above the transition temperatures (Fig. 7). The inset of Fig. 7 illustrates the magnetization/demagnetization curves for the samples $x = 0.00, 0.21$ and 0.42 (as an example of the curves from which the data are obtained). A similar trend is observed for both types of hysteresis. From Table 1, an increase of the Si content for higher Cr doped samples (from $x = 0.42$) is observed, which can be related to the presence of the α -Fe phase. This higher Si content can also affect the hysteresis for that set of samples, though the non-monotonic feature remains unaltered as the Si content is the same for samples up to $x = 0.35$.

The upper panel of Fig. 8 shows the temperature dependence of ΔS_T for the $\text{LaFe}_{11.6-x}\text{Cr}_x\text{Si}_{1.4}$ series, together with the Cr content dependence of the peak values ($|\Delta S_T^{max}|$) (inset), for a magnetic field change of 1.9 T measured upon cooling. It is observed that the temperatures at which $|\Delta S_T^{max}|$ takes place, i.e transition temperatures, decrease with Cr content (as previously observed). An evident increase in the width of ΔS_T curves for higher Cr content is also observed. $|\Delta S_T^{max}|$ decreases as Cr content increases following a power law of the form $f(x) = a + bx^c$, being x the Cr content (with $a = 22.1(5)$ J kg $^{-1}$ K $^{-1}$, $b = -69(10)$ J kg $^{-1}$ K $^{-1}$ and $c = 2.6(3)$). For low Cr content, $|\Delta S_T^{max}|$ remains practically constant, with changes being noticeable for $x \approx 0.25$ and above. With respect to the shape of the ΔS_T vs. T curves, the characteristic abrupt variation associated to FOPT MC materials is observed for compositions up to $x = 0.47$. The lower panel of Fig. 8 shows the temperature dependence of ΔT_S and the Cr dependence of ΔT_S^{max} (inset) for a magnetic field change of 1.9 T measured upon cooling. The same main features observed for the ΔT case are also observed for $\Delta T_S(T)$. The ΔT_S response

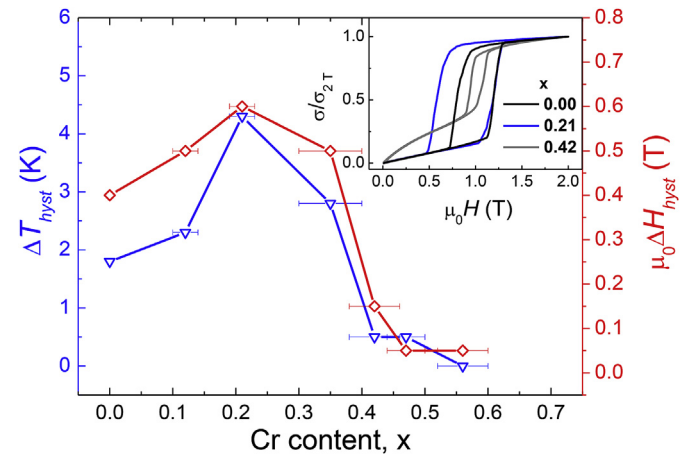


Fig. 7. Thermal and magnetic hysteresis associated to the $\text{LaFe}_{11.6-x}\text{Cr}_x\text{Si}_{1.4}$ series. Inset: Magnetization/demagnetization curves at temperatures close to T_{trans} for $x = 0.00, 0.21$ and 0.42 samples.

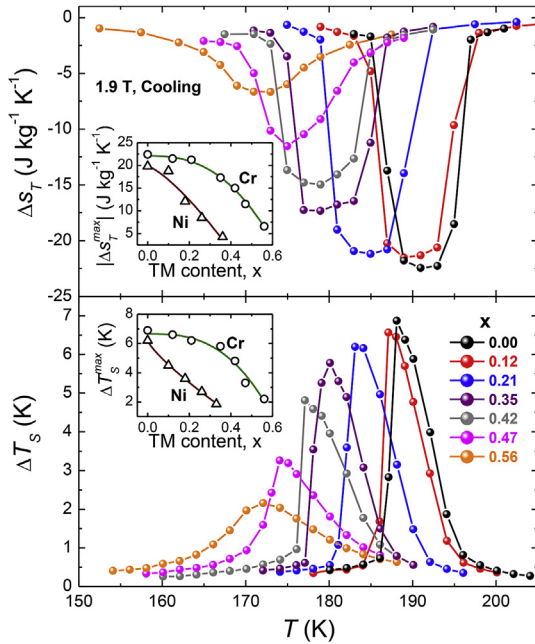


Fig. 8. Temperature dependence while cooling of ΔS_T (upper panel) and ΔT_S (lower panel) for a magnetic field change of 1.9 T for the $\text{LaFe}_{11.6-x}\text{Cr}_x\text{Si}_{1.4}$ series. Insets: $|\Delta S_T^{\max}|$ and ΔT_S^{\max} as a function of the Cr content, compared to Ni doped results [13].

decrease and also shifts to lower temperatures with Cr addition. The curves become wider for higher Cr concentration. The decrease of ΔT_S^{\max} with Cr content can be phenomenologically fitted to a power law of the form $f(x) = a + bx^c$ (with $a = 6.7(4)$ K, $b = -10(3)$ K and $c = 2.8(7)$), as seen in the inset. Regarding the adiabatic temperature change, similar $\Delta T_S(T)$ curve shape of $x = 0.00$ sample is retained up to $x = 0.47$.

The results are compared to those of Ni-containing $\text{La}(\text{Fe}, \text{Si})_{13}$ compounds [13], showing the evolution of $|\Delta S_T^{\max}|$ and ΔT_S^{\max} with increasing Ni concentration in the insets of Fig. 8. Ni doping produces a significantly larger decrease of the magnetocaloric response than Cr doping. This is in contrast with the smaller variation of the average magnetic moment per atom in the case of the Ni-doped alloy. DFT calculations indicate that Ni atoms are coupled with a magnetic moment of $0.44 \mu_B$ while $-1.5 \mu_B$ is obtained for Cr atoms. This demonstrates that to understand the role of the TM doping on the MC response, the characteristics of the phase transition has to be characterized. For this purpose, two MC field dependence analyses had been applied [12,22]. These methods had been reported to easily determine the order of the phase transition and the critical SOPT-FOPT composition. With a quantitative magnitude, they identify the FOPT character of various materials, such as $\text{La}(\text{Fe}, \text{Si})_{13}$ [13], Heusler alloys [44] or cobaltites [45]. Moreover, these analyses do not require any fitting procedure or extended data calculations.

One of these methods recently reports [22] that an overshoot of n values larger than 2 is observed near the transition temperature for FOPT (while for SOPT, n goes to a minimum at Curie transition, increasing to values not beyond 2 thereafter). Fig. 9 shows the temperature dependence of the field dependence exponent n for a magnetic field change of 1.9 T for the $\text{LaFe}_{11.6-x}\text{Cr}_x\text{Si}_{1.4}$ series. It is observed a clear overshoot of n above 2 for samples up to $x = 0.47$, indicating that samples undergoes a FOPT. For $x = 0.56$, a smooth variation from a minimum value up to 2 is observed, indicating SOPT-behavior [46]. The values of the overshoot can give us information about the nature of the transition, whereby higher values

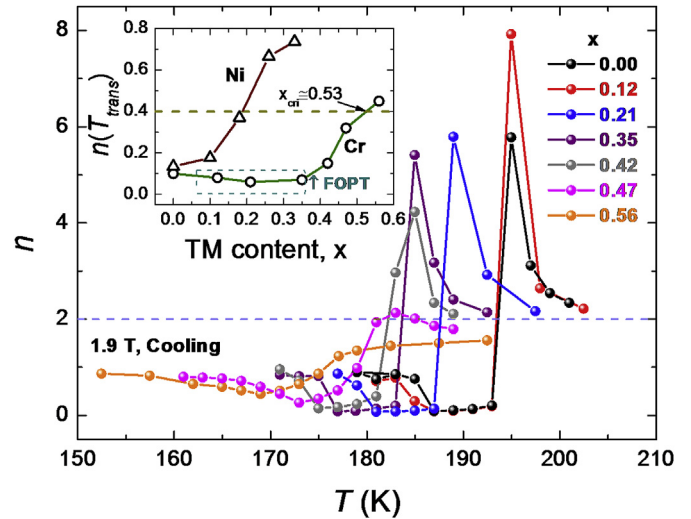


Fig. 9. Temperature dependence of the field dependence exponent n for a magnetic field change of 1.9 T for the $\text{LaFe}_{11.6-x}\text{Cr}_x\text{Si}_{1.4}$ series. Inset: $n(T_{\text{trans}})$ as a function of the Cr content for 1.9 T, compared to Ni doped results [13].

are attained with increasing FOPT-character, though a very fine analysis should be performed as the temperature step can affect the obtained characteristics (the narrow peak should be characterized with enough temperature resolution). It should be noted that these overshoots are found to appear for temperatures near the transition and for moderate magnetic fields, i.e. when the itinerant-electron metamagnetic transition occurs.

On the other hand, it was shown [12] that the values of the exponent n at the transition temperatures (T_{trans}) are related to the order of the phase transition, being $n(T_{\text{trans}}) < 0.4$ for FOPT, $n(T_{\text{trans}}) > 0.4$ for SOPT and $n(T_{\text{trans}}) = 0.4$ for the critical SOPT-FOPT point (where FOPT crossovers to SOPT). The inset of Fig. 9 shows $n(T_{\text{trans}})$ as a function of the Cr content for the $\text{LaFe}_{11.6-x}\text{Cr}_x\text{Si}_{1.4}$, indicating FOPT for samples up to $x = 0.47$ and SOPT for $x = 0.56$ sample. This is in agreement with the results obtained with the previously mentioned overshoot method. Interpolating $n(T_{\text{trans}}) = 0.4$ for the critical point, it is estimated that the critical composition corresponds to a Cr content of $x = 0.53$, which is larger than the previously reported for similar compounds (a 120% increase [24]). For comparison, the evolution of $n(T_{\text{trans}})$ with Ni concentration is also shown in the inset of Fig. 9. It can be observed that Ni content affects the order of the phase transition in a larger way that for Cr doping, changing rapidly the order of the phase transition from first to second order, with a critical SOPT-FOPT composition $x \approx 0.21$ [13]). Further analysis of the Bean-Rodbell model [47], which is considered a good approximation to describe $\text{La}(\text{Fe}, \text{Si})_{13}$ compounds [19], shows that $n(T_{\text{trans}})$ is smaller when the FOPT-character is stronger (which is described by the η parameter in the model). According to this, it is observed that for samples with $x = 0.12, 0.21$ and 0.35 , their $n(T_{\text{trans}})$ values are lower than that of the parent compound, indicating a stronger FOPT-behavior (as highlighted by the dashed box). This is not observed for the Ni doped series, where a monotonous change from first to second order is obtained. The obtained results are in excellent agreement with the hysteresis evolution observed for these series of compounds, obtaining the maximum hysteresis for the smallest $n(T_{\text{trans}})$ value (i.e. $x = 0.21$ sample). As already discussed, the slightly higher Si content for higher Cr-doped samples can slightly modify this tendency though it has to be accounted that for all the compounds the Si content is below the critical limit found at 1.65 [12].

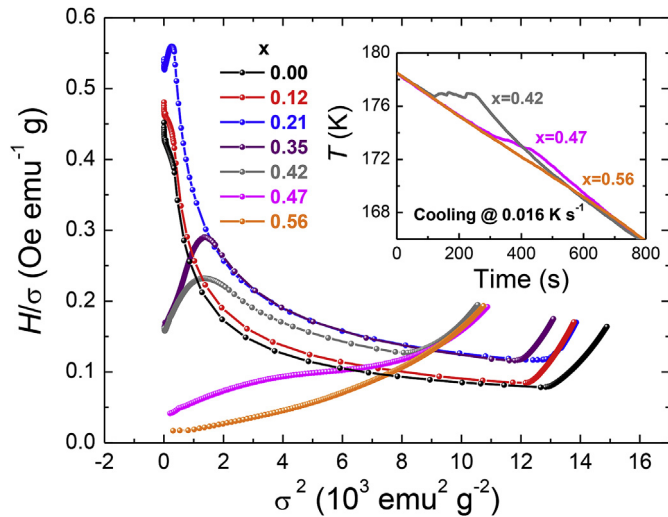


Fig. 10. Arrott plots for the $\text{LaFe}_{11.6-x}\text{Cr}_x\text{Si}_{1.4}$ series at selected temperatures close to their transitions. Inset: Sample temperature while cooling at constant rate at temperatures close the transition for $x = 0.42, 0.47$ and 0.56 samples.

In addition, the Banerjee's criterion is applied to compare with the results previously obtained by the MC field dependence analyses [23]. This criterion, based on mean field assumptions, establishes that negative slopes of isothermal H/σ vs. σ^2 (Arrott plots [48]) indicate FOPT, while positive slopes point to SOPT. Fig. 10 shows the Arrott plots for the $\text{LaFe}_{11.6-x}\text{Cr}_x\text{Si}_{1.4}$ series at selected temperatures close to their transitions. The extracted results show good agreement to the MC field dependence analyses except for $x = 0.47$ sample, which is supposed to undergoes a SOPT according to the Banerjee's criterion. One should note that this compound has a composition very near to the critical FOPT-SOPT composition for the studied series ($x = 0.53$ from the previous analyses). However, for $x = 0.47$ sample, the shape of the curves hint at an inflection point, which is not observed for the $x = 0.56$ (more in agreement with the expected SOPT-behavior described by the model). This can indicate the existence of a slight FOPT-character though the Banerjee's criterion does not allow more information to be obtained. It should be noted that Banerjee's criterion imposes a mean field approximation, which might not represent properly the material under study, leading to erroneous interpretations [49]. Moreover, for MC analysis there is no contribution arising from impurities (as their transition temperatures are well separated to the 1:13 phase one) but for Banerjee's criterion the results can be affected if the contribution of the impurity phase to the magnetic moment is significant [50]. Some works also reported contradictory results to Banerjee's criterion in compounds that do not follow a mean field model [51].

Another way to determine the order of the phase transition is using calorimetry studies. In this work, the sample temperature inside the direct magnetocaloric measurement setup was monitored while the chamber temperature was modified at a constant rate. For FOPT, a plateau region is attained (the sample temperature remains constant during the transition) while for SOPT a gradual evolution of the sample temperature can be found. The inset of Fig. 10 shows the sample temperature while cooling at 0.016 K s^{-1} for $x = 0.42, 0.47$ and 0.56 samples (the samples closer to the critical FOPT-SOPT composition). A plateau is observed for both $x = 0.42$ and 0.47 samples (though it is smoother for the latter as it is closer to the critical point), indicating FOPT. On the other hand, for $x = 0.56$ sample, a continuous evolution is observed (a slight slope change can be observed at the transition temperature), indicating

SOPT. These results are in agreement with those obtained from the MC field dependence analysis, confirming the accuracy of the method (but differ from those of the Banerjee's criterion).

4. Conclusions

Using Cr-doped $\text{La}(\text{Fe},\text{Si})_{13}$ series, we have shown that the magnetocaloric response of a series of materials can remain constant even if the magnetic moment of the sample decreases significantly. The explanation of this peculiar behavior is the change of the nature of the phase transition, becoming more first order for low Cr content. Unlike other transition metal dopants, Cr substitutes Fe–I (8b) sites, and has a large solid solubility limit. By using novel magnetocaloric criteria to determine the order of phase transition, a non-monotonic evolution of the FOPT-character is found for increasing Cr additions. This feature is accompanied by a variation of the thermal and magnetic hysteresis. DFT calculations support the experimental microstructural and magnetic results. They also further reveal the antiferromagnetic coupling of Cr to Fe.

Acknowledgements

This work was supported by AEI/FEDER-UE (project MAT-2016-77265-R) and the PAI of the Regional Government of Andalucía. L. Moreno-Ramírez acknowledges a FPU fellowship from the Spanish MEC. O.G., I.R., and K.S. acknowledge funding by the DFG in the framework of the priority program "Ferroic Cooling" (SPP1599). The work of F. Maccari was supported by the German Research Foundation within the Priority Program SPP 1959. The authors thankfully acknowledge the computer resources and technical assistance provided by the Red Española de Supercomputación (RES) at the Marenostrum supercomputer (Project QCM-2018-3-0037).

References

- [1] V. Franco, J.S. Blázquez, J.J. Ipus, J.Y. Law, L.M. Moreno-Ramírez, A. Conde, Magnetocaloric effect: From materials research to refrigeration devices, *Progress in Materials Science* 93 (2018) 112–232.
- [2] M. Balli, S. Jandl, P. Fournier, A. Kedous-Lebouc, Advanced materials for magnetic cooling: Fundamentals and practical aspects, *Applied Physics Reviews* 4 (2) (2017), 021305.
- [3] A. Fujita, S. Fujieda, Y. Hasegawa, K. Fukamichi, Itinerant-electron meta-magnetic transition and large magnetocaloric effects in $\text{La}(\text{Fe}_x\text{Si}_{1-x})_{13}$ compounds and their hydrides, *Physical Review B* 67 (10) (2003) 104416.
- [4] J. Liu, J.D. Moore, K.P. Skokov, M. Krautz, K. Löwe, A. Barcza, M. Katter, O. Gutfleisch, Exploring $\text{La}(\text{Fe},\text{Si})_{13}$ -based magnetic refrigerants towards application, *Scripta Materialia* 67 (6) (2012) 584–589.
- [5] J. Lyubina, R. Schäfer, N. Martin, L. Schultz, O. Gutfleisch, Novel Design of $\text{La}(\text{Fe},\text{Si})_{13}$ Alloys Towards High Magnetic Refrigeration Performance, *Advanced Materials* 22 (33) (2010) 3735–3739.
- [6] I.A. Radulov, D.Y. Karpenkov, K.P. Skokov, A.Y. Karpenkov, T. Braun, V. Brabänder, T. Gottschall, M. Pabst, B. Stoll, O. Gutfleisch, Production and properties of metal-bonded $\text{La}(\text{Fe},\text{Mn},\text{Si})_{13}\text{H}_x$ composite material, *Acta Materialia* 127 (2017) 389–399.
- [7] M.Q. Huang, W.E. Wallace, M.E. McHenry, Q. Chen, B.M. Ma, Soft magnetic properties of LaCo_{13} and $\text{La}(\text{Co},\text{Fe})_{13}$ alloys, *Journal of Applied Physics* 83 (11) (1998) 6471–6473.
- [8] G. Jaeger, The Ehrenfest Classification of Phase Transitions: Introduction and Evolution, *Archive for History of Exact Sciences* 53 (1) (1998) 51–81.
- [9] O. Gutfleisch, T. Gottschall, M. Fries, D. Benke, I. Radulov, K.P. Skokov, H. Wende, M. Gruner, M. Acet, P. Entel, M. Farle, Mastering hysteresis in magnetocaloric materials, *Philosophical Transactions of the Royal Society A* 374 (2074) (2016).
- [10] M.F.J. Boeije, M. Maschek, X.F. Miao, N.V. Thang, N.H. van Dijk, E. Brück, Mixed magnetism in magnetocaloric materials with first-order and second-order magnetoelastic transitions, *Journal of Physics D: Applied Physics* 50 (17) (2017) 174002.
- [11] K.G. Sandeman, Magnetocaloric materials: The search for new systems, *Scripta Materialia* 67 (6) (2012) 566–571.
- [12] V. Franco, J.Y. Law, A. Conde, V. Brabänder, D.Y. Karpenkov, I. Radulov, K. Skokov, O. Gutfleisch, Predicting the tricritical point composition of a series of LaFeSi magnetocaloric alloys via universal scaling, *Journal of Physics D: Applied Physics* 50 (41) (2017) 414004.
- [13] L.M. Moreno-Ramírez, C. Romero-Muñiz, J.Y. Law, V. Franco, A. Conde,

- I.A. Radulov, F. Maccari, K.P. Skokov, O. Gutfleisch, The role of Ni in modifying the order of the phase transition of $\text{La}(\text{Fe}, \text{Ni}, \text{Si})_{13}$, *Acta Materialia* 160 (2018) 137–146.
- [14] M. Krautz, K. Skokov, T. Gottschall, C.S. Teixeira, A. Waske, J. Liu, L. Schultz, O. Gutfleisch, Systematic investigation of Mn substituted $\text{La}(\text{Fe}, \text{Si})_{13}$ alloys and their hydrides for room-temperature magnetocaloric application, *Journal of Alloys and Compounds* 598 (2014) 27–32.
- [15] M. Katter, V. Zellmann, G.W. Reppel, K. Uestuener, Magnetocaloric properties of $\text{La}(\text{Fe}, \text{Co}, \text{Si})_{13}$ bulk material prepared by powder metallurgy, *IEEE Transactions on Magnetics* 44 (2008) 3044.
- [16] M.Q. Huang, W.E. Wallace, R.T. Obermyer, S. Simizu, M. McHenry, S.G. Sankar, Magnetic characteristics of $\text{RCo}_{13-x}\text{Si}_x$ alloys (R=La, Pr, Nd, Gd, and Dy), *Journal of Applied Physics* 79 (8) (1996) 5949–5951.
- [17] T. Lei, K.K. Nielsen, K. Engelbrecht, C.R.H. Bahl, H. Neves Bez, C.T. Veje, Sensitivity study of multi-layer active magnetic regenerators using first order magnetocaloric material $\text{La}(\text{Fe}, \text{Mn}, \text{Si})_{13}\text{H}_y$, *Journal of Applied Physics* 118 (1) (2015), 014903.
- [18] J.D. Moore, K. Morrison, K.G. Sandeman, M. Katter, L.F. Cohen, Reducing extrinsic hysteresis in first-order $\text{La}(\text{Fe}, \text{Co}, \text{Si})_{13}$ magnetocaloric systems, *Applied Physics Letters* 95 (25) (2009) 252504.
- [19] H.N. Bez, K.K. Nielsen, P. Norby, A. Smith, C.R.H. Bahl, Magneto-elastic coupling in $\text{La}(\text{Fe}, \text{Mn}, \text{Si})_{13}\text{H}_y$ within the Bean-Rodbell model, *AIP Advances* 6 (5) (2016), 056217.
- [20] M. De Graef, M.E. McHenry, *Structure of Materials*, 1st Edition ed., Cambridge University Press, Cambridge, 2007.
- [21] F. Wang, A. Kurbakov, G.-J. Wang, F.-X. Hu, B.-G. Shen, Z.-H. Cheng, Strong interplay between structure and magnetism in $\text{LaFe}_{11.3}\text{Co}_{0.6}\text{Si}_{1.1}$: A neutron diffraction study, *Physica B: Condensed Matter* 385–386 (2006) 343–345.
- [22] J.Y. Law, V. Franco, L.M. Moreno-Ramírez, A. Conde, D.Y. Karpinkov, I. Radulov, K.P. Skokov, O. Gutfleisch, A quantitative criterion for determining the order of magnetic phase transitions using the magnetocaloric effect, *Nature Communications* 9 (1) (2018) 2680.
- [23] B.K. Banerjee, On a generalised approach to first and second order magnetic transitions, *Physics Letters* 12 (1) (1964) 16–17.
- [24] S.T. Zong, Y. Long, The influence of Cr and Ni on the character of magnetic phase transition in $\text{LaFe}_{11.52-x}\text{M}_x\text{Si}_{1.48}$ alloys, *AIP Advances* 8 (4) (2017), 048101.
- [25] J. Liu, T. Gottschall, K.P. Skokov, J.D. Moore, O. Gutfleisch, Giant magnetocaloric effect driven by structural transitions, *Nature Materials* 11 (2012) 620.
- [26] L. Tocado, E. Palacios, R. Burriel, Entropy determinations and magnetocaloric parameters in systems with first-order transitions: Study of MnAs, *Journal of Applied Physics* 105 (9) (2009), 093918.
- [27] B. Kaeswurm, V. Franco, K.P. Skokov, O. Gutfleisch, Assessment of the magnetocaloric effect in $\text{La}, \text{Pr}(\text{Fe}, \text{Si})$ under cycling, *Journal of Magnetism and Magnetic Materials* 406 (2016) 259–265.
- [28] V. Franco, J.S. Blázquez, A. Conde, Field dependence of the magnetocaloric effect in materials with a second order phase transition: A master curve for the magnetic entropy change, *Applied Physics Letters* 89 (22) (2006) 222512.
- [29] G. Kresse, J. Furthmüller, Efficient iterative schemes for ab initio total-energy calculations using a plane-wave basis set, *Physical Review B* 54 (16) (1996) 11169–11186.
- [30] M.E. Gruner, W. Keune, B. Roldan Cuenya, C. Weis, J. Landers, S.I. Makarov, D. Klar, M.Y. Hu, E.E. Alp, J. Zhao, M. Krautz, O. Gutfleisch, H. Wende, Element-Resolved Thermodynamics of Magnetocaloric $\text{LaFe}_{13-x}\text{Si}_x$, *Physical Review Letters* 114 (5) (2015), 057202.
- [31] M.E. Gruner, W. Keune, J. Landers, S. Salamon, M. Krautz, J. Zhao, M.Y. Hu, T. Toellner, E.E. Alp, O. Gutfleisch, H. Wende, Moment-Volume Coupling in $\text{La}(\text{Fe}_{1-x}\text{Si}_x)_{13}$, *physica status solidi (b)* 255 (2) (2018) 1700465.
- [32] P.E. Blöchl, Projector augmented-wave method, *Physical Review B* 50 (24) (1994) 17953–17979.
- [33] G. Kresse, D. Joubert, From ultrasoft pseudopotentials to the projector augmented-wave method, *Physical Review B* 59 (3) (1999) 1758–1775.
- [34] J.P. Perdew, K. Burke, M. Ernzerhof, Generalized Gradient Approximation Made Simple, *Physical Review Letters* 77 (18) (1996) 3865–3868.
- [35] H.J. Monkhorst, J.D. Pack, Special points for Brillouin-zone integrations, *Physical Review B* 13 (12) (1976) 5188–5192.
- [36] S.H. Vosko, L. Wilk, M. Nusair, Accurate spin-dependent electron liquid correlation energies for local spin density calculations: a critical analysis, *Canadian Journal of Physics* 58 (8) (1980) 1200–1211.
- [37] S.T. Zong, C.L. Wang, Y. Long, B. Fu, J.M. Shi, J. Han, Y.Y. Zhao, Solid solubility in 1:13 phase of doping element for $\text{La}(\text{Fe}, \text{Si})_{13}$ alloys, *AIP Advances* 6 (5) (2016), 056223.
- [38] M. Rosca, M. Balli, D. Fruchart, D. Gignoux, E.K. Hlil, S. Miraglia, B. Ouladidaf, P. Wolfers, Neutron diffraction study of $\text{LaFe}_{11.31}\text{Si}_{1.69}$ and $\text{LaFe}_{11.31}\text{Si}_{1.69}\text{H}_{1.45}$ compounds, *Journal of Alloys and Compounds* 490 (1) (2010) 50–55.
- [39] A. Fujita, H. Yako, Stability of metallic, magnetic and electronic states in NaN_{13} -type $\text{La}(\text{Fe}, \text{Si}_{1-x})_{13}$ magnetocaloric compounds, *Scripta Materialia* 67 (6) (2012) 578–583.
- [40] T.T.M. Palstra, J.A. Mydosh, G.J. Nieuwenhuys, A.M. van der Kraan, K.H.J. Buschow, Study of the critical behaviour of the magnetization and electrical resistivity in cubic $\text{La}(\text{Fe}, \text{Si})_{13}$ compounds, *Journal of Magnetism and Magnetic Materials* 36 (3) (1983) 290–296.
- [41] G. Zsolt, Magnetic coupling in transition-metal-doped $\text{LaSiFe}_{11.5}\text{TM}_{0.5}$ (TM=Cr, Mn, Co and Ni), *Europhysics Letters* 110 (4) (2015) 47006.
- [42] F. Wang, Y.F. Chen, G.J. Wang, B.G. Shen, The effect of Mn substitution in $\text{LaFe}_{11.7}\text{Si}_{1.3}$ compound on the magnetic properties and magnetic entropy changes, *Journal of Physics D: Applied Physics* 36 (1) (2002) 1–3.
- [43] K. Löwe, J. Liu, K. Skokov, J.D. Moore, H. Sepehri-Amin, K. Hono, M. Katter, O. Gutfleisch, The effect of the thermal decomposition reaction on the mechanical and magnetocaloric properties of $\text{La}(\text{Fe}, \text{Si}, \text{Co})_{13}$, *Acta Materialia* 60 (10) (2012) 4268–4276.
- [44] J.Y. Law, A. Díaz-García, L.M. Moreno-Ramírez, V. Franco, A. Conde, A.K. Giri, How concurrent thermomagnetic transitions can affect magnetocaloric effect: The $\text{Ni}_{49-x}\text{Mn}_{36-x}\text{In}_{15}$ Heusler alloy case, *Acta Materialia* 166 (2019) 459–465.
- [45] J.Y. Law, V. Franco, A. Conde, S.J. Skinner, S.S. Pramana, Modification of the order of the magnetic phase transition in cobaltites without changing their crystal space group, *Journal of Alloys and Compounds* 777 (2019) 1080–1086.
- [46] V. Franco, A. Conde, Scaling laws for the magnetocaloric effect in second order phase transitions: From physics to applications for the characterization of materials, *International Journal of Refrigeration* 33 (3) (2010) 465–473.
- [47] C.P. Bean, D.S. Rodbell, Magnetic Disorder as a First-Order Phase Transformation, *Physical Review* 126 (1) (1962) 104–115.
- [48] A. Arrott, J.E. Noakes, Approximate Equation of State For Nickel Near its Critical Temperature, *Physical Review Letters* 19 (14) (1967) 786–789.
- [49] S. Bustingorry, F. Pomiro, G. Aurelio, J. Curiale, Second-order magnetic critical points at finite magnetic fields: Revisiting Arrott plots, *Physical Review B* 93 (22) (2016) 224429.
- [50] M. Sánchez-Pérez, L.M. Moreno-Ramírez, V. Franco, A. Conde, M. Marsilius, G. Herzer, Influence of nanocrystallization on the magnetocaloric properties of Ni-based amorphous alloys: Determination of critical exponents in multi-phase systems, *Journal of Alloys and Compounds* 686 (2016) 717–722.
- [51] C.M. Bonilla, J. Herrero-Albillos, F. Bartolomé, L.M. García, M. Parra-Borderías, V. Franco, Universal behavior for magnetic entropy change in magnetocaloric materials: An analysis on the nature of phase transitions, *Physical Review B* 81 (22) (2010) 224424.